Directional Epitaxial Crystallization and Tentative Crystal Structure of Poly(9,9′-di-*n*-octyl-2,7-fluorene)

Martin Brinkmann†

Institut Charles Sadron, 6, rue Boussingault, 67083 Strasbourg, France

Received June 22, 2007; Revised Manuscript Received July 24, 2007

ABSTRACT: Directional epitaxial crystallization is used to prepare highly oriented films of poly(9,9′-di-*n*-octyl-2,7-fluorene) (PFO). This orientation method implies the use of a crystallizable aromatic solvent (1,3,5-trichlorobenzene) playing successively the role of the solvent for PFO for $T > 63$ °C and the role of an orienting substrate below this temperature. Extended areas of the oriented PFO can be formed on a given substrate after simple evaporation of the crystallized solvent under vacuum. The effect of annealing on the thin film structure and morphology was followed by transmission electron microscopy (TEM) in bright field and dark field modes and atomic force microscopy. Upon annealing, oriented crystalline PFO lamellae and axialites are formed by coalescence of smaller nanocrystalline domains. As shown by electron diffraction, a single-crystal-like structure is formed after a short annealing of the as-oriented films at 210 °C and slow cooling (0.5 °C/min) to room temperature. The films consist of oriented lamellar crystals in edge-on orientation on the SiO_2 substrate, and the PFO chains are oriented parallel to the TCB stacking direction (c_{TCB}). The reflection rules deduced from various selected area electron diffraction (SAED) patterns obtained by rotation-tilt indicate that PFO crystallizes in an orthorhombic structure with $Pnb2_1$ space group. A tentative crystal structure was obtained from the simulations of the SAED patterns and molecular modeling. The epitaxial relationship at the PFO/TCB interface suggests that 1D epitaxy is involved: the PFO chains are oriented parallel to the stacking direction of TCB (*c*-axis); the 3.95 Å distance between TCB molecules matches closely the reticular distance of 4.1 Å corresponding to dense planes of *n*-octyl side groups of interdigitated PFO chains.

I. Introduction

The crystallization of flexible polymer chains, e.g., polyolefins, has attracted a wealth of efforts and research activity over the past few decades. More rigid systems, e.g., semiconducting polymers like regioregular poly(3-alkylthiophene)s, substituted poly(*p*-phenylenevinylene)s, and polyfluorenes, are only recently receiving attention regarding their crystallization. This is justified by the need to establish the relationships between structure, morphology, and electronic properties in order to optimize the performances of electronic and optoelectronic devices (organic field effect transistors, organic light-emitting diodes) which are based on these polymers.[1−3] Poly(9,9-di-*n*-octyl-2,7-fluorene) (PFO) is a high-efficiency blue-emitting polymer,[4,5] with potential applications for the fabrication of polarized light-emitting diodes (PLED's)[6,7] or electrically pumped organic lasers.[8] Concerning the structure of PFO, photophysical studies have evidenced two different PFO backbone conformations, namely α and β, whose occurrences depend closely on the preparation method of the samples, e.g., annealing or solvent vapor exposure.[9−14] It has been reported that the β-type conformation prevails in PFO thin films exposed to vapors of good solvents, e.g., toluene. The α chain conformation, which is mainly observed in the glassy state and annealed thin films ($T = 135$ °C), is believed to be more disordered and to have a less planar backbone than the β conformation.[9] The α vs β conformation of the PFO chain is very much related to the reversible order−disorder transition (ODT) observed around $T = 80$ °C between the crystalline and the polymer liquid crystalline (PLC) phase.[10] The exact β-type polymer chain conformation is still unknown. On the basis of studies using transmission electron microscopy and X-ray diffraction, Chen et al. have proposed an orthorhombic crystal structure of PFO involving eight polymer chains and a space group $P2_12_12_1$.[14] The latter author suggested that the conjugated backbone of the PFO chains is not planar. The dihedral angles between successive fluorene monomers was found in the range 15°−24°.[14]

Concerning charge transport, Redecker et al. have demonstrated that relatively high charge carrier mobilities (up to 8.5×10^{-3} cm^2/(V s)) can be reached once the PFO is oriented in its nematic phase ($T > 160$ °C).[15] In its liquid crystalline phase, PFO can be readily oriented on rubbed polyimide substrates.[16,17] More recently, Yase and co-workers have shown that highly oriented PFO thin films can be obtained by a friction transfer method[18] similar to that initially proposed by Wittmann and Smith for the preparation of oriented poly(tetrafluoroethylene) (PTFE) thin films.[19] These oriented PFO layers were used for the fabrication of PLEDs with an integrated polarization ratio of 31 and a high luminance reaching 300 Cd/m^2.[6] All these results clearly show that the orientation of conjugated polymers is an essential step toward the improvement of optical and charge transport properties and controlled fabrication of PLEDs.

An alternative method for the orientation of semiconducting π-conjugated polymers has been recently demonstrated in the case of regioregular poly(3-hexylthiophene) (P3HT).[20,21] Directional epitaxial crystallization of P3HT from a solution in a crystallizable aromatic solvent (1,3,5-trichlorobenzene) (TCB) allows to prepare extended areas of highly oriented P3HT on glass or SiO_2 substrates.[20,21] The principle of this method relies on the twofold role of TCB: (i) for $T > T_m$ (T_m is the melting temperature of TCB), TCB acts as the solvent of the polymer, and (ii) for $T < T_m$ TCB plays the role of the nucleating and orienting surface for the epitaxial orientation of the polymer. We further demonstrated that directional epitaxial crystallization allows to prepare highly oriented films of various P3HT samples with different molecular weights in the range 7.3−70 kDa.[21] In particular, we have shown that P3HT with $M_w \geq 18.8$ kDa

† E-mail: brinkman@ics.u-strasbg.fr.

10.1021/ma071390d CCC: $37.00
Published on Web 09/12/2007

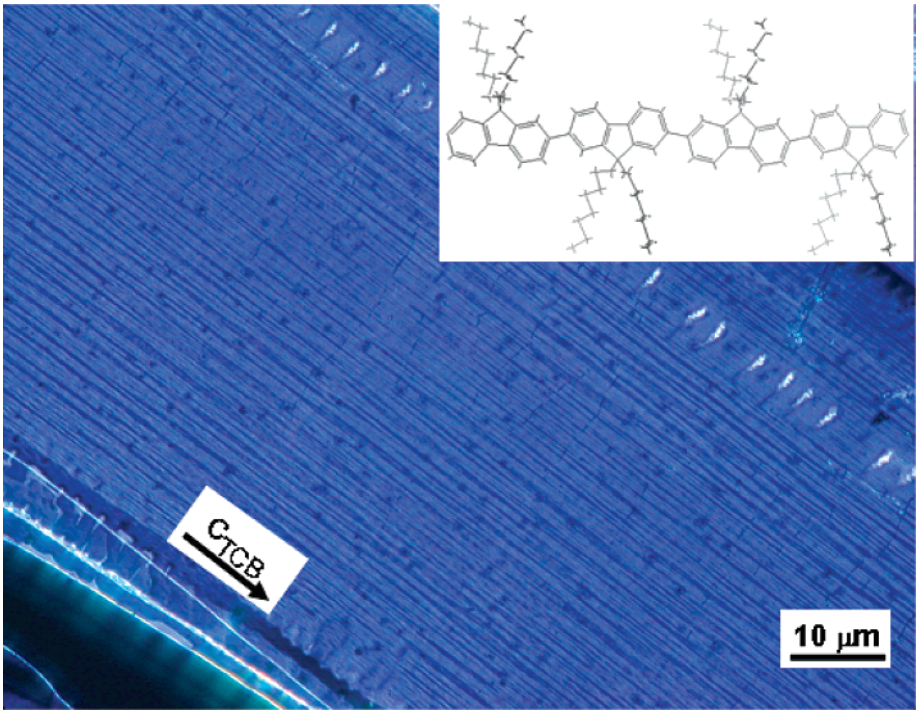

Figure 1. Optical microscopy image (with crossed polarizers) of an oriented thin film of PFO grown by directional epitaxial crystallization in TCB. The inset depicts a sequence of four monomers of a PFO chain having a planar 2_1 zigzag conformation of the conjugated backbone.

crystallizes like a classical semicrystalline polymer with the alternation of crystalline lamellae separated by amorphous interlamellar zones containing chain folds, chain ends, and tie molecules whereas for $M_w \leq 7.3$ kDa, P3HT crystallizes like an oligomer without chain folding.[21]

Herein, it is demonstrated that the mechanism of epitaxial crystallization of PFO in TCB leads to highly oriented thin films. Moreover, annealing of the oriented films followed by slow cooling improves drastically the orientation level which becomes very similar to that obtained by the friction transfer method of Yase et al.[18] Annealing is observed to result in the coalescence of small nanodomains which are already crystalline and oriented so as to form extended lamellar domains but without clear indication for the existence of amorphous interlamellar zones. These highly crystalline films are perfectly suited to perform rotation-tilt TEM experiments in order to determine more precisely the crystal structure of PFO. Molecular modeling combined with simulations of the SAED patterns allowed us to propose a tentative model of the PFO crystal structure.

II. Experimental Section

The PFO sample was synthesized using the method published in the literature.[22] The weight-average molecular mass (M_w) obtained from GPC (polystyrene standard) was ca. 104 kDa with a polydispersity index of 2.95. For the directional solidification of PFO, TCB was used as a crystallizable solvent. As described previously for regioregular poly(3-hexylthiophene),[20,21] the preparation of oriented PFO films involves three main steps: First, a thin film of PFO is prepared by drop-casting (1 wt % solution in chloroform) onto a clean glass slide (Corning 2947). 10−25 mg of TCB powder is deposited onto the PFO film and sandwiched between the PFO-coated glass slide and a clean glass coverslip. The whole is placed on a hot bar with a temperature gradient (Koeffler bench) and heated at temperatures slightly above T_m until melting of TCB occurs. At this stage, TCB dissolves the solid film of PFO and an almost colorless and slightly blue fluorescent solution of PFO forms and spreads uniformly between the glass slide and the coverslip. The system is then slowly moved on the Koeffler bench toward the colder part, until directional crystallization of TCB occurs. The appearance of a yellow color in the films indicates that PFO crystallizes subsequently to TCB. Finally, after removing the coverslip, TCB is slowly evaporated at room temperature under primary vacuum (10^{-2} mbar) for 1 h, leaving large areas (~1 mm^2) of the oriented PFO film on the glass substrate. From AFM measurements, the thickness of the remaining PFO film is in the range 30−100 nm. Thin films of PFO were also grown onto freshly cleaved mica substrates.

For TEM analysis, the oriented areas were identified by optical microscopy (Leica DMR-X microscope (see Figure 1)). Annealing was performed by using a THMS-600 hot stage (Linkam) connected to a TMS-94 temperature controller. Prior to annealing under nitrogen, the chamber of the hot stage was purged several times with the inert gas. Typical annealing procedures were as follows: first the sample was annealed to a temperature of 210 °C at a heating rate of 30 °C/min and left at this temperature for a variable time in the range 10 min−1 h. This annealing step was followed by a slow cooling to room temperature at a rate of 0.5 °C/min.

For TEM observations, the PFO films were coated with a thin amorphous carbon film, and the PFO/carbon film was removed from the glass substrate by dipping the films into an aqueous HF solution (5 wt %). The PFO/carbon layers were subsequently recovered onto TEM copper grids. TEM was performed in bright field, dark field, and rotation-tilt configurations on a CM12 Philips microscope equipped with a MVIII CCD camera (Soft Imaging Systems). The surface topography of PFO thin films was investigated by atomic force microscopy (AFM) with a Nanoscope III in tapping mode using Si tips (25−50 N/m and 280−365 kHz). Image treatments (FFT) were performed by using AnalySIS (Soft Imaging System) software.

Molecular modeling was performed on a Silicon Graphic station using the Cerius2 program. A trial-and-error procedure was used to refine the crystal structure of PFO. The detailed methodology for the structure refinement is described in section III.4.

III. Results and Discussion

(1) Structure of the As-Oriented PFO Thin Films. Let us first consider the morphology and the structure of the as-oriented PFO thin films. Figure 1 shows an optical microcopy image of a highly oriented PFO thin film oriented by directional epitaxial

solidification in TCB. Under crossed polarizers, the films are highly birefringent. Their morphology is fibrilar with a fiber axis oriented parallel to the *c*-axis of the TCB crystals (c_{TCB}). The maximum of optical absorbance is observed when the vibrational direction of the incident light is oriented parallel to the fiber direction of the films, indicating that the PFO chain axis c_{PFO} is parallel to c_{TCB}, i.e., $c_{PFO}||c_{TCB}$. The fibrous morphology is further demonstrated by AFM, as seen in Figure 2. The electron diffraction pattern of the oriented films shows four intense reflections: one very intense meridional reflection at 0.41 nm and three strong equatorial reflections at 0.66, 0.43, and 0.33 nm. The 0.41 nm reflection corresponds to half the length of the fluorene monomer unit and suggests that neighboring PFO chains are translated parallel to the chain axis by half the length of the fluorene monomer unit, leading to an interdigitated configuration of the *n*-octyl side chains. This 0.41 nm reflection shows a typical arcing, indicative of an azimuthal misorientation of the PFO domains in the plane of the substrate.

A close look at the film morphology by AFM shows some remarkable features. Indeed, as seen in the phase mode AFM image in Figure 2c, the PFO fibers are formed by small nanodomains (average size ~50 nm) that are separated by very clear "grain boudaries". This observation reminds of the nanodomains observed by Chen and co-workers inside lamellar crystalline domains of PFO by scanning electron microscopy.[11] When analyzing the morphology closer, we observe a substructure inside the nanocrystallites as illustrated in the phase mode image of Figure 3. This substructure gives rise to an alternation of stripes in the phase mode image with a typical width of ~10 nm, the stripes being oriented parallel to the PFO chain axis direction. The origin of this substructure is not yet clear. It may correspond to the coexistence of small domains with slightly different structures, e.g., domains with PFO chains in α and β conformations.

(2) Effect of Annealing on the Thin Film Structure and Morphology. Annealing is known to affect dramatically the PFO thin film structure and morphology.[9−14] In order to determine the effect of annealing on the oriented PFO thin films, we have annealed them at 210 °C for various times, followed by slow cooling to room temperature (0.5 °C/min).

The films annealed for 10 min at 210 °C exhibit a higher briefringence than the as-oriented films, indicating that the overall orientation and crystallinity in the films is substantially improved. Figure 4a shows a typical AFM topographic image of the thin film morphology observed after such an annealing. The films exhibit a succession of lamellar domains 100−200 nm wide whose edges are oriented roughly perpendicular to the average PFO chain direction. From the section profile of the lamellae, step heights with a characteristic value of 1.2 ± 0.4 nm are measured. The latter value is close to both the *a* and *b* parameters of the PFO unit cell ($a = 2.56$ nm, $b = 2.34$ nm[11]). Interestingly, we observe very often the emergence of a terrace growing out of an underying one. This observation suggests the presence of edge dislocations, i.e., that successive terraces are generated in the direction perpendicular to the substrate (*a*-axis) by edge dislocations oriented perpendicular to the chain axis.

The lamellar morphology of the PFO films is also observed by TEM in bright field mode (Figure 4b) with similar dimensions of the lamellae as obtained by AFM. In the present case, the crystalline lamellae of PFO are observed in an edge-on orientation. Interestingly, the lamellae are separated one from another by bright and relatively sharp boundary lines, and the edges of the lamellae are not sharp but fluctuate very much.

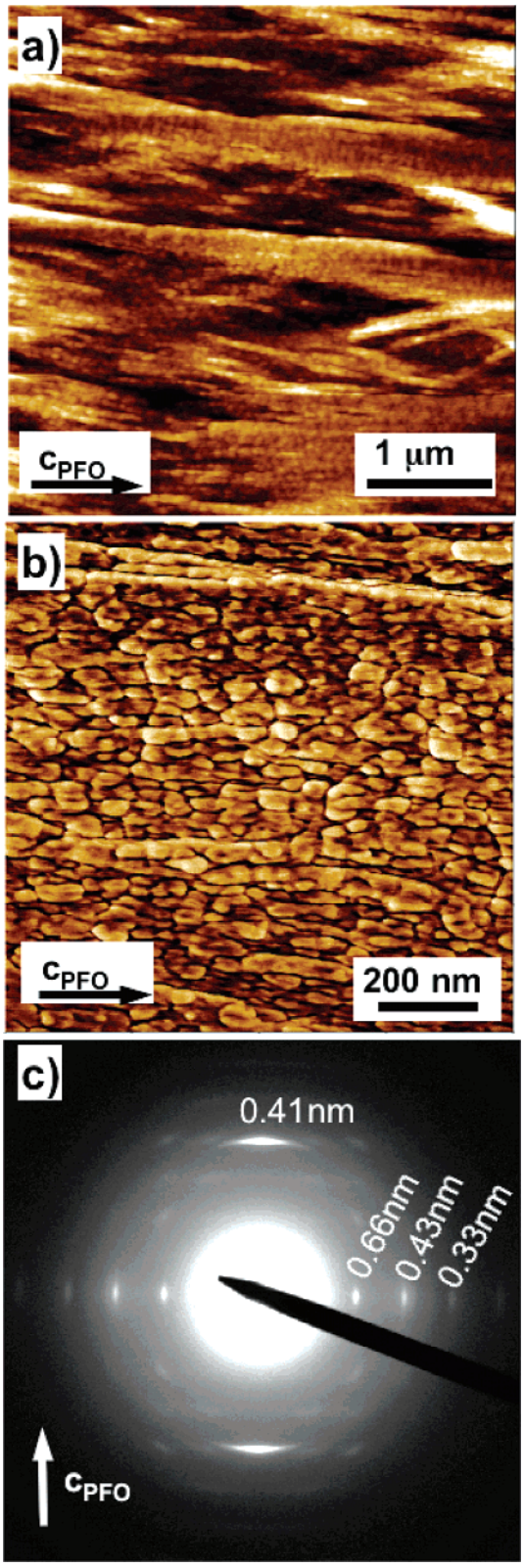

Figure 2. (a) AFM topography of an oriented PFO thin film grown by directional epitaxial crystallization in TCB, (b) enlarged AFM phase mode image of an oriented area showing nanocrystalline domains, and (c) electron diffraction pattern.

Figure 5 shows the electron diffraction pattern and the defocused diffraction image of such an oriented and annealed PFO film. The lamellar domains are oriented with their edges perpendicular to the chain orientation, which coincides with the c_{TCB} direction (white arrows in Figure 4a). The dark field (DF) image shown

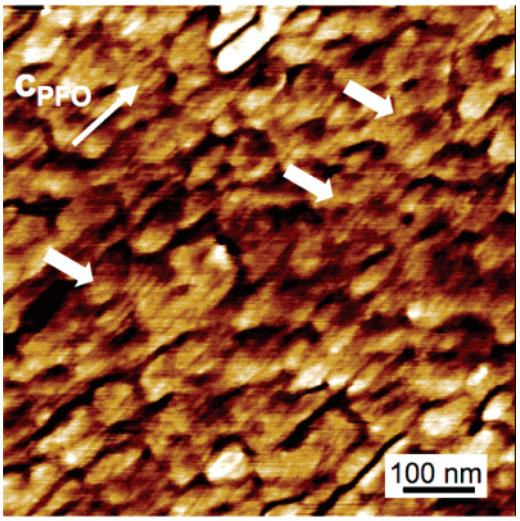

Figure 3. Phase mode AFM image showing the substructure inside the PFO nanodomains in as-oriented PFO films grown by directional epitaxial crystallization. The PFO chain direction is indicated by an arrow.

in Figure 4c was obtained by selecting the strongest meridional reflection (0.41 nm) in the SAED pattern. The DF shows the characteristic succession of lamellar domains separated by narrow and dark boundary lines. Contrary to the case of oriented P3HT thin films,[20] the DF does not give any clear evidence for extended interlamellar amorphous zones between successive crystalline lamellar domains. This means that PFO lamellar domains are separated by narrow grain boundaries which appear as dark and bright lines in the DF and BF images, respectively. The absence of extended amorphous interlamellar zones between the crystalline lamellae reflects the higher rigidity of the PFO chain as compared to regioregular P3HT. Apparently, the more rigid PFO chains are not able to fold like P3HT. The present morphology reminds the extended chain lamellae usually observed for polyethylene grown under high pressure[23] or in the case of rigid conjugated systems like P-4-BCMU (poly-{5,7-dodecadiyne-1,12-diol bis[((4-butoxycarbonyl)methyl)urethane]}).[24,25] In the present case, the crystalline lamellae are observed in an edge-on orientation.

The average extended chain length obtained for $DP_n \sim 90$ and a monomer repeat length of 0.83 nm amounts to ~75 nm, which is close to, but smaller than, the average lamellar width measured from the BF and AFM images in Figure 4. Significant fluctuations in the lamellar width as well as the presence of lamellar tapering are clearly seen in the DF image of Figure 4c. These two observations may be attributed to the conjunction of (i) a large molecular weight distribution of the PFO chains (PDI = 2.95) and (ii) intralamellar segregation of PFO chains as a function of their molecular weight. A similar lamellar tapering has been observed in oriented thin films on rubbed polyimide substrates of the parent compound poly(9,9-bis(2-ethylhexyl)-fluorene-2,7-diyl).[26] We propose that the intralamellar segregation of PFO chains as a function of their molecular weight may be favored by the very slow cooling of the samples from 210 °C to RT, underlining the importance of the kinetics of thermal annealing on the resulting structure and morphology of lamellar domains.

Prolonged annealing at $T = 210$ °C for 1 h results in further interesting modifications of the film morphology. Under crossed polarizers, the films exhibit a maximum of birefringence at 45° orientation of c_{PFO} with respect to the polarizer, indicating that the preferential orientation induced by epitaxial crystallization

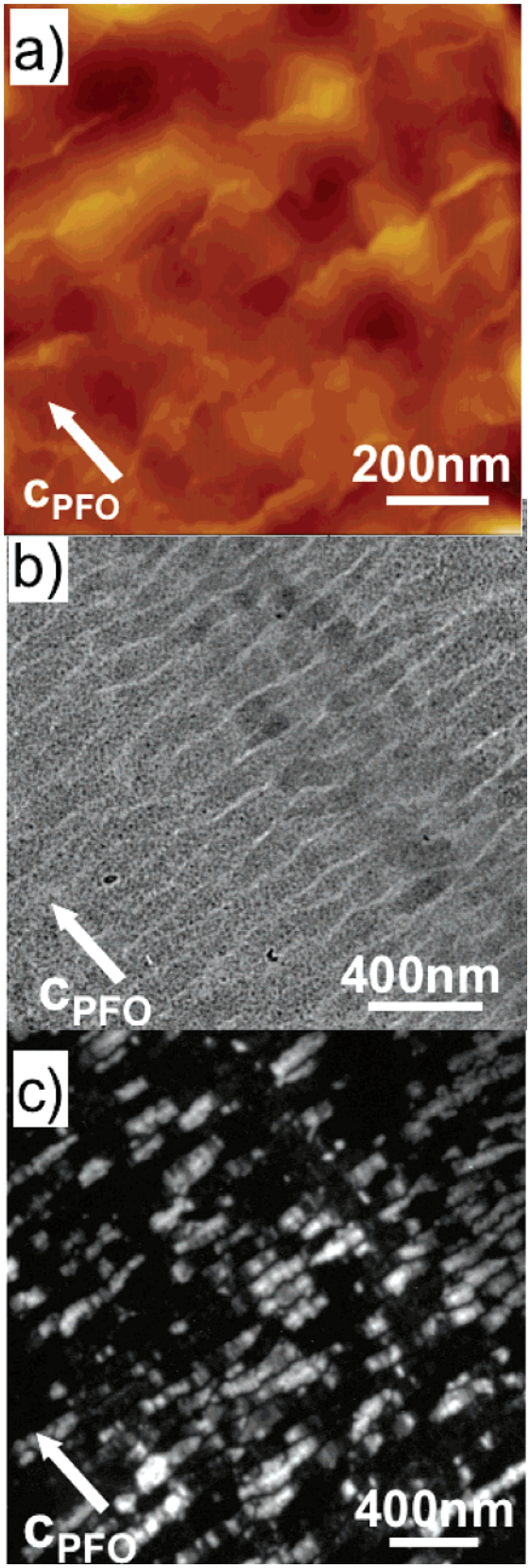

Figure 4. (a) Bright field (BF) TEM image of an oriented PFO thin film after annealing at 210 °C and slow cooling to room temperature at 0.5 °C/min. (b) AFM topographic image. The PFO chain direction is indicated by an arrow. (c) Dark field image corresponding to diffracted electrons of the most intense 0.415 nm reflection (see Figure 5).

($c_{PFO}||c_{TCB}$) is maintained. Contrary to earlier suggestions, annealing of the PFO films at 210 °C is not sufficient to

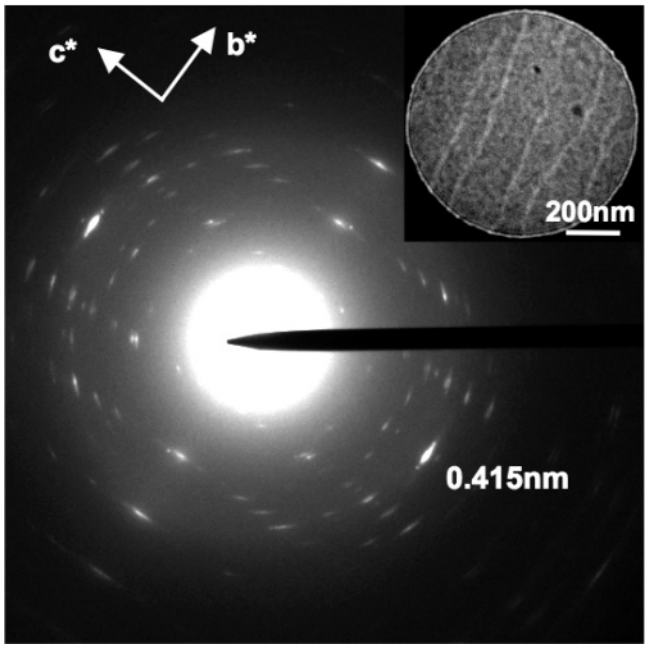

Figure 5. Electron diffraction pattern of a PFO thin film oriented by directional epitaxial crystallization in TCB and subsequently annealed at 210 °C (10 min) and slowly cooled to RT at 0.5 °C/min. The inset corresponds to the defocused diffraction image in proper relative orientation to the electron diffraction pattern and corresponding to the diffracting area.

eliminate the processing history of oriented samples.[11−14] As seen in Figure 6a, optical microscopy in phase contrast reveals lozenge-shaped domains and sectors. The sectors range from 5 to 20 μm in size and the obtuse angle has a characteristic and constant value in the range 132°−139°. Within the lozenge-shaped domains, we observe a regular and periodic striped substructure. These striped domains are observed to radiate out of well-defined nucleation centers (marked by white arrows in Figure 6), but they tend to remain oriented perpendicular to the average PFO chain axis direction. The average width of the stripes amounts to ∼0.5−1.0 μm, whereas their apparent length reaches 10−20 μm. The stripes are oriented essentially perpendicular to the PFO chain direction. Further details concerning the morphology are obtained by AFM. The AFM topographic and phase mode images (Figure 6b,c) provide a close look at the surface of the domains and reveal the origin of the periodic striped morphology. Inside the lozenge-shaped domains, elongated and faceted domains form a "factory roof" type of structure. The faceting periodicity is in the range 500−800 nm, in good agreement with the stripe periodicity obtained by optical microscopy. The slope of the factory roof structure is small and does not exceed 5°. The surface of the facets shows a terraced structure similar to the one observed for a shorter annealing time with similar step heights. In polyethylene, similar topographies have been described as corrugations.

The typical morphology of Figure 6 differs from the classical spherulite because of the uniform birefringence observed within the lozenge-shaped domains, which results from the uniform *c*-axis orientation within the domains. The structures here resemble more the axialites observed by Chen and co-workers[13] but with one important difference. In the PFO axialites, the *c*-axis direction rotates progressively in-plane when moving from the center to the exterior of the axialites. This is not observed in the present case because the initial orientation of the PFO chains is maintained by epitaxy via the TCB substrate.

(3) Space Group Determination. In an earlier report, Chen et al. have proposed for the crystal structure of PFO a unit cell with space group $P2_12_12_1$.[11] This space group determination was based on a single SAED pattern corresponding to the [0 0 1] zone of a PFO domain. Whereas the unit cell parameters determined by Chen et al. are in agreement with those determined from our ED patterns (only a slighly shorter *c*-axis of 3.24 nm is observed in our case), the additional diffraction evidence gathered in the present investigation makes it possible to refine more precisely the space group of the crystal structure by using additional SAED patterns. To do so, we have prepared PFO thin films with different orientations on various substrates, keeping the processing history identical. Using the cell parameters of the orthorhombic unit cell by Chen et al., it is possible to index the SAED pattern in Figure 5 obtained for a thin film grown on a TCB substrate. This pattern is characteristic of the [1 0 0] zone. Crystalline PFO films with a different orientation were prepared by drop-casting on a freshly cleaved mica substrate followed by annealing at 210 °C and slow cooling (0.5 °C/min) to RT. As seen in Figure 7, it was possible to find areas corresponding to the characteristic [0 0 1] zone that yield SAED patterns identical to those obtained by Chen et al. for PFO films on glass substrate.[11]

The carefull examination of the SAED pattern of Figure 7 yields following reflection rules:

$$h\,0\,0: \qquad h = 2n \tag{1}$$

$$0\,k\,0: \qquad k = 2n \tag{2}$$

Assuming that the extended PFO chain has a planar zigzag 21 helical conformation (see inset in Figure 1), Chen et al. assumed the additional reflection rule:

$$0\,0\,l: \qquad l = 2n \tag{3}$$

The authors concluded that PFO crystallizes in an orthorhombic unit cell with $P2_12_12_1$ space group and with eight PFO chains per cell. In fact, reflection rule (3) is observed in the electron diffraction pattern corresponding to the [1 0 0] zone. Indeed, in Figure 7b we observe the absence of 0 0 *l* reflections with odd values of *l*. The SAED pattern in Figure 7b allows to identify one additional reflection rule. Indeed, in this projection, we observe the absence of (0 *k l*) layer lines with odd values of *k*. Hence, the additional reflection condition can be written as

$$0\,k\,l: \qquad k = 2n \tag{4}$$

This additional reflection rule suggests a space group different from the one intially proposed by Chen et al.[11] The two first space groups which are compatible with all four reflection rules listed above are $C222_1$ and $Pnb2_1$.[27] The $C222_1$ space group implies one additional reflection rule, namely, *h k* 0 reflections with $h + k = 2n$. As seen from Figure 7, this selection rule is not observed in the SAED pattern corresponding to the [0 0 1] zone. Hence, this space group can be discarded. The space group $Pnb2_1$ implies also one additional reflection rule, namely

$$h\,0\,l: \qquad h + l = 2n \tag{5}$$

To check whether this reflection rule applies, it would be necessary to prepare samples with a standing *b*-axis orientation. Unfortunately, we did not manage to obtain the standing *b*-axis orientation. To rule out the space groups with a higher symmetry than $Pnb2_1$, we recorded additional projections using a rotation-tilt stage in order to verify the absence of additional reflection rules concerning general *h k l* reflections. Typically, we tilted

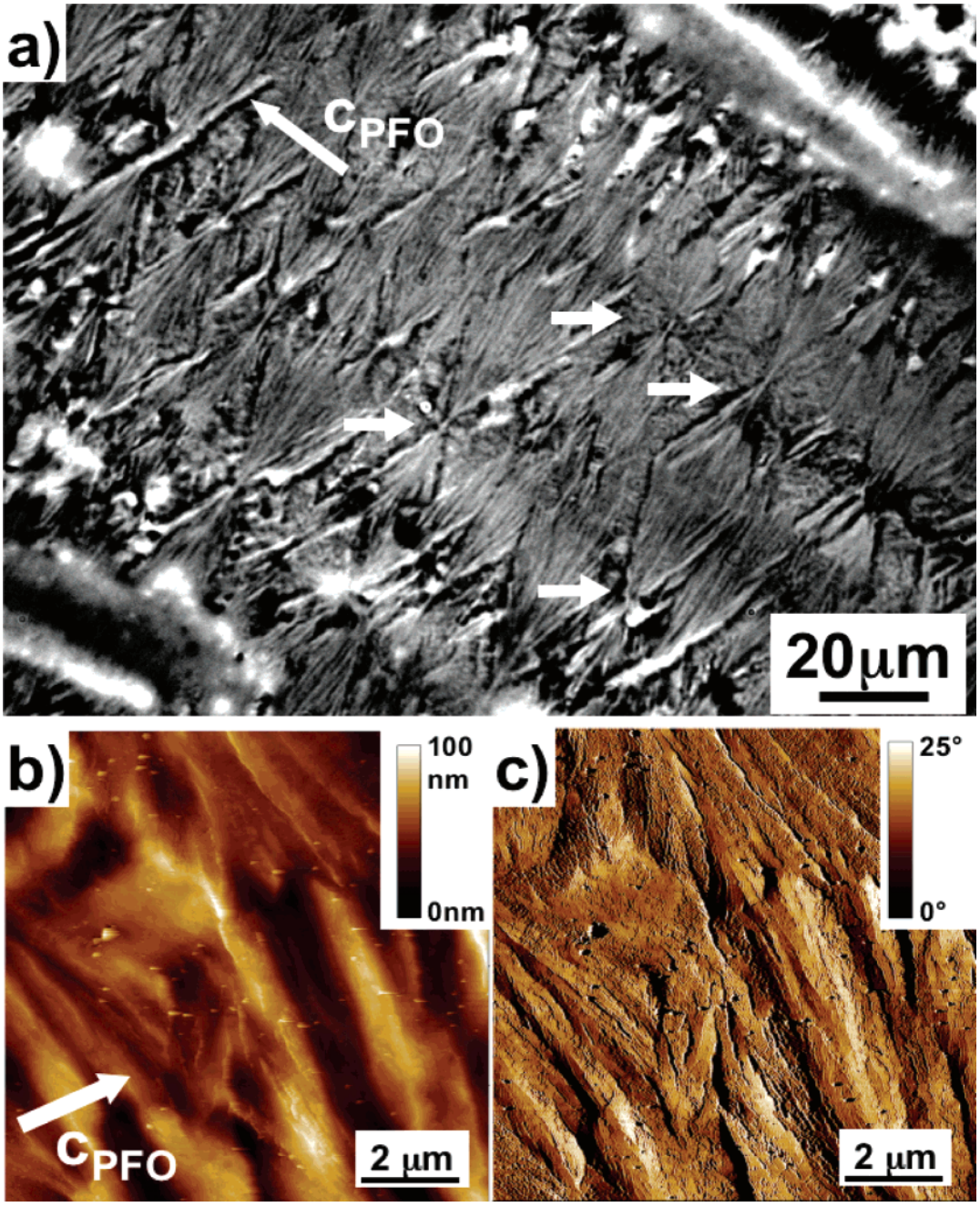

Figure 6. (a) Phase contrast optical microscopy image obtained for a PFO thin film grown by directional epitaxial crystallization and subsequently annealed at $T = 210$ °C for 1 h and slowly cooled to RT (0.5 °C/min). Corresponding topographic (b) and phase mode (c) images of the annealed PFO thin film.

the oriented samples either around the *c*-axis or around the *b*-axis and recorded characteristic projections at specific tilt angles. When rotated around the chain axis direction (*c*-axis), a representative projection is obtained for a tilt angle $\theta_c = 42 \pm 1°$ (Figure 8). Using the unit cell parameters of the orthorhombic cell, we indexed the most intense reflections and found that this projection is characteristic of the [1 1 0] zone. The expected tilt angle of 42°, calculated from the unit cell parameters of the orthorhombic structure, matches perfectly the experimental tilt angle. When tilted around the *a*-axis, a characteristic projection was observed for a tilt angle of $18 \pm 1°$. The observed ED pattern corresponds to the [4 0 −1] zone. Considering the SAED patterns of the [1 1 0] and the [4 0 −1] zones, we could not identify additional reflection rules for the general *h k l* reflections, supporting the identification of $Pnb2_1$ as the most probable space group. As shown in the following, this space group accounts for all the observed SAED patterns.

(4) Tentative Molecular Model of the Crystal Structure of PFO. The main pieces of information related to the identification of the $Pnb2_1$ space group are the following. The unit cell contains four symmetry-related positions. Accordingly, in order to generate eight PFO chains in the cell, one must consider a structural unit made of two PFO chains. When constructing this two-chain unit, the strong intensity of the (0 0 8) reflection suggests that the two PFO chains are translated by half the monomer repeat length along the PFO chain direction. Now the question arises: what distinguishes the two PFO chains of the pattern? Two main possibilities may be considered. The first possibility, initially suggested by Chen et al., is that the conjugated backbone of the PFO chains bears some intrinsic helicity, giving the possibility to distinguish left-

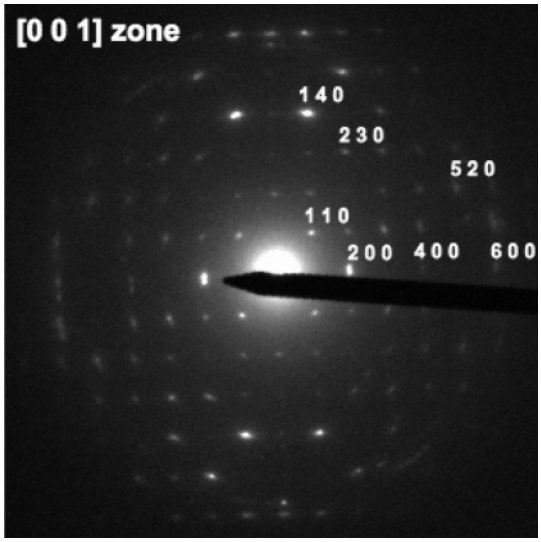

Figure 7. SAED pattern obtained for a PFO thin film grown on a mica substrate. Using the orthorhombic structure, it can be indexed as the [0 0 1] zone.

and right-handed PFO chains.[11] A twisting angle of 144° between the planes of successive fluorene moieties has been evidenced experimentally in various fluorene-based oligomers,[28,29] and a 5_2-helix was identified for the parent compound poly(9,9-bis(2-ethylhexyl)-fluorene-2,7-diyl) from the analysis of a X-ray diffraction fiber pattern.[26] However, the presence of a 5_2-helix can be excluded in the present case from the carefull analysis of the [1 0 0] zone SAED pattern in Figure 8. Moreover, a helical structure of the PFO backbone is difficult to reconcile with an ordered crystal packing of the *n*-octyl side chains. As a matter of fact, the structure by Chen et al. lacks any ordered packing of alkyl side chains. We were thus led to use a different approach. We do not calculate *a priori* a backbone conformation for an isolated PFO chain and build the crystal, but rather we consider that the crystallization of PFO is controlled to a large extent by the organization and crystal packing of the *n*-octyl side chains which can enforce the planarization of the conjugated backbone. In other words, the conformation calculated for an isolated PFO chain is believed to be significantly different from that of a PFO chain in the crystal, contrary to what is usually observed for more classical polymers, e.g., polyolefins. The possibility to observe either planar or helical conformations of the polyfluorene backbone, depending on the structure of the alkyl side chains, is not really surprising. A similar dependence has been evidenced in poly(di-*n*-alkylsilane)s. For instance, poly(di-*n*-butylsilane) and poly(di-*n*-pentylsilane) are observed to adopt a 73 helical conformation,[30] whereas poly(diethylsilane) and poly(di-*n*-hexylsilane) are almost always observed in a near-planar conformation.[31]

In the present case, the fact that the length of the *c*-axis equals four fluorene residues implies that the twist between successive fluorene monomers in the chain equals $n\pi/2$ (n is an integer). In agreement with earlier reports,[9,10] the most probable conformation of the PFO backbone in the crystalline structure is believed to be the planar zigzag conformation illustrated in the inset of Figure 1. A planar backbone conformation does however not exclude the possbility for handedness of the PFO chain as a whole. In Figure 9, we depict the conformation of the "tetraradial" PFO chain obtained by optimization of the molecular geometry but imposing a planar conjugated backbone.[32] The two *n*-octyl side chains of a given fluorene monomer have different conformations and confer handedness to the whole PFO chain. It is thus possible to distinguish both left- and right-handed PFO chains for the tetraradial conformation.

A second possibility for the structure of the two-chain unit can be the presence of a typical pairing of two chains into a tightly interdigitated dimer-like structure. In such a pair of PFO chains, the chains are likely to be linked through a symmetry operation such as an inversion center. In the following, we have decided, admittedly somewhat arbitrarily, to consider a pair of PFO chains related through an inversion center and with a relative shift along the *c*-axis by half the length of the monomer unit, i.e., 0.41 nm to obtain an interdigitated pattern. Morevoer, for the sake of simplicity, we have restricted our investigations to both the tetraradial and the biradial conformations of the lateral *n*-octyl side chains, as depicted in Figure 9. Similar molecular conformations were proposed by Winokur et al. for poly(di-*n*-alkylsilane)'s, e.g., poly(di-*n*-butylsilane).[33] In the case of the tetraradial configuration, we have considered that the side chains can be inclined with respect to the orientation of the polyfluorene backbone, as suggested by the results of Grell et al. using computer simulations on a 9,9-dioctylfluorene monomer.[9] In the case of the tetraradial configuration, the *n*-octyl side chains are fixed in an all-trans conformation.

A first set of positions for the PFO chains in the unit cell was obtained by considering a fluorene polymer chain with a planar zigzag conformation (21 helix, see inset in Figure 1) without *n*-octyl side chains. The polyfluorene chains are oriented parallel to the *c*-axis. Once the best agreement between calculated and experimental SAED pattern corresponding to the [0 0 1] zone was obtained for the simplified polyfluorene chains, the *n*-octyl side chains were added to the conjugated fluorene backbone. The refinement of the structure was obtained by successively optimizing (i) the agreement between calculated and experimental SAED patterns of the [1 0 0], [0 0 1], [1 1 0], and [4 0 −1] zones and (ii) minimizing the number of close contacts in the unit cell. An iterative trial-and-error method was implemented by modifying at each step the positions of the two PFO chains of the dimer in the unit cell. In Figure 10, we depict the calculated SAED patterns for the [1 0 0], [0 0 1], [1 1 0], and [4 0 −1] zones giving the best agreement with the experimental patterns. As a matter of fact, the best agreement was obtained for the tetraradial conformation of the PFO chains. The refined crystal structure is illustrated in Figure 11, which shows the *c*-axis projection as well as the interdigitation of the *n*-octyl side chains in the PFO "dimer".

The first remark is that the simulated patterns do indeed reproduce the positions of the observed layer lines in the different SAED patterns, supporting the proposed space group. Second, even though a few short contacts are present in the structure, we observe globaly a very good correspondence between the intensities of the calculated and the simulated patterns. This is particularly true for the intensities of the reflections in the calculated ED pattern for the [1 0 0] zone which are matching very well those in the observed SAED pattern (see Figure 8). Concerning the [0 0 1] zone, the most intense (2 0 0), (1 4 0), and (5 2 0) reflections are nicely reproduced in the calculated pattern. For the [1 1 0] zone, the strong (0 0 8), (−1 1 0), and (−3 3 0) reflections are well reproduced. Of course, the agreement between calculated and experimental SAED patterns is not perfect. Discrepancies between calculated and experimental ED patterns are mainly visible for the [1 1 0] and the [4 0 −1] zones. They underline both the limitations of the present approach based on a rotation-tilt experiment and the important structural complexity of the PFO chains. In particular, the present analysis cannot identify

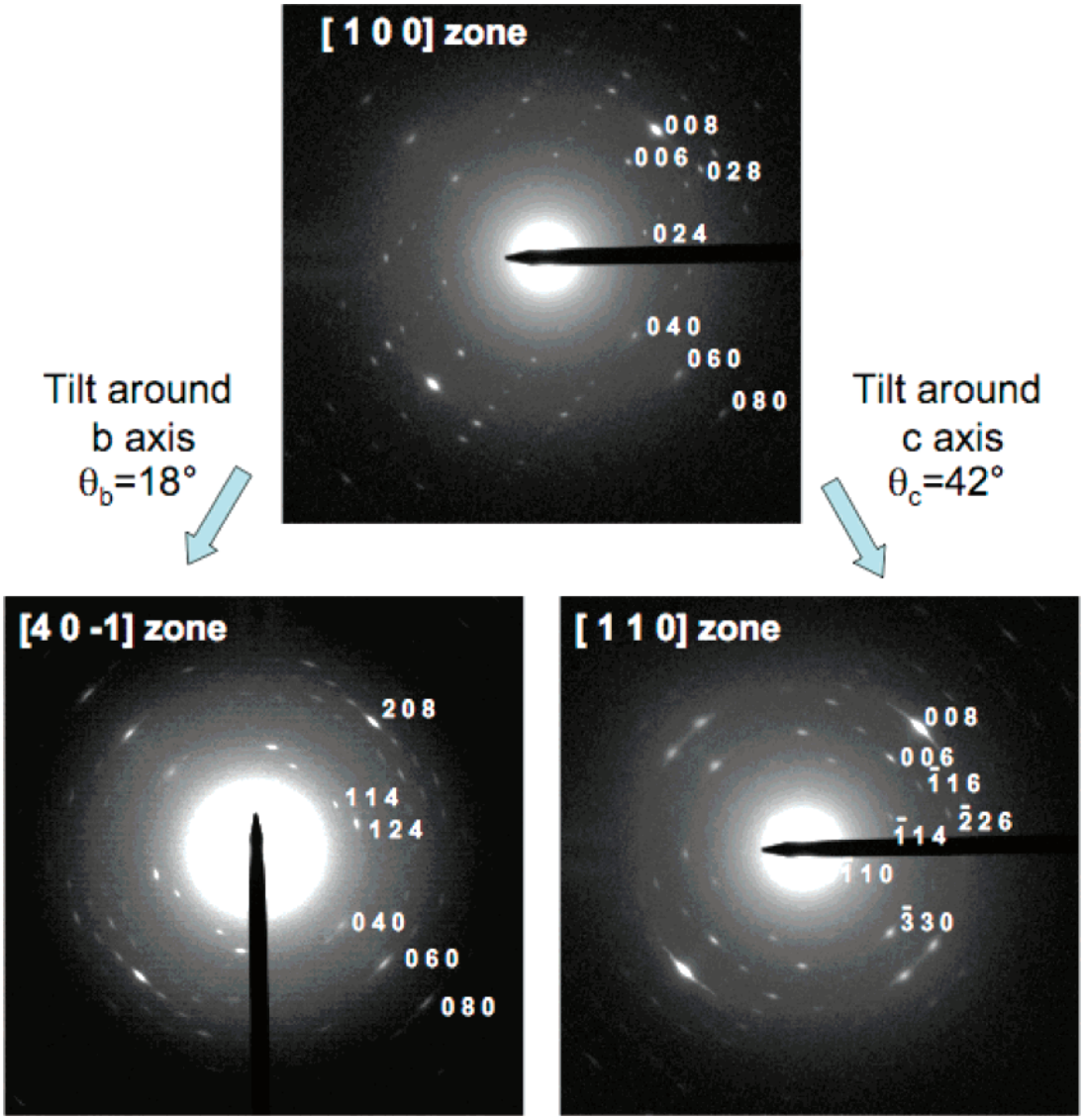

Figure 8. Rotation-tilt experiment on a PFO thin film grown by epitaxial directional crystalliation and subsequent annealing at 210 °C (10 min) and slow cooling (0.5 °C/min). The [4 0 −1] zone is obtained for a tilt $\theta_b = 18°$ around the *b*-axis. The [1 1 0] zone is obtained for a tilt $\theta_c = 42°$ around the *c*-axis.

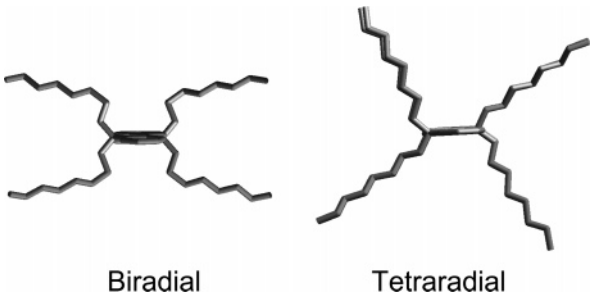

Figure 9. Projections of the PFO chain conformation along the *c*-axis for the biradial and tetraradial configuration of the *n*-octyl side chains. The hydrogen atoms have been omitted for the sake of clarity.

a possible departure from a perfectly planar backbone conformation of the PFO chains in the crystal.

Even though the present crystal structure is clearly tentative, the comparison with the crystal structure proposed by Chen et al. is instructive. First, the helical conformation of the PFO backbone assumed by Chen et al. clearly prevents an efficient packing of the *n*-octyl side chains. Instead, looking at the 0 0 1 projection of our model, we can observe a preferential orientation of the *n*-octyl side chains along the *a*- and *b*-axes

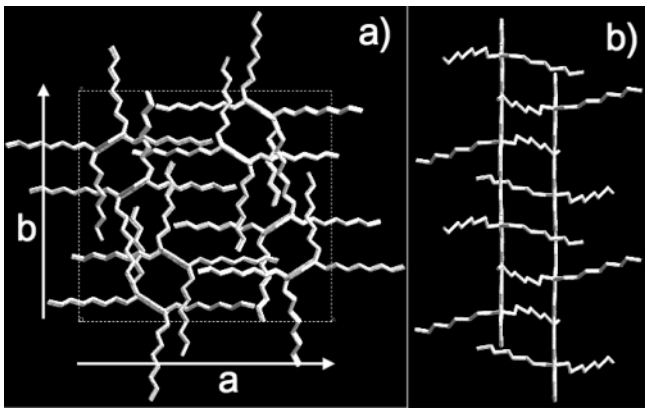

Figure 10. (a) *c*-axis projection of the refined PFO crystal structure. The hydrogen atoms are not shown for the sake of clarity. (b) Projection of the two-chain pattern along the [1 −1 0] direction.

of the unit cell. Interestingly, the unit cell of PFO contains four groups of PFO "dimers". The two PFO chains of a dimer share the same handedness, and the planes of their conjugated backbones are parallel one to another. The distance between the PFO backbones of the two chains in the dimer motif amounts

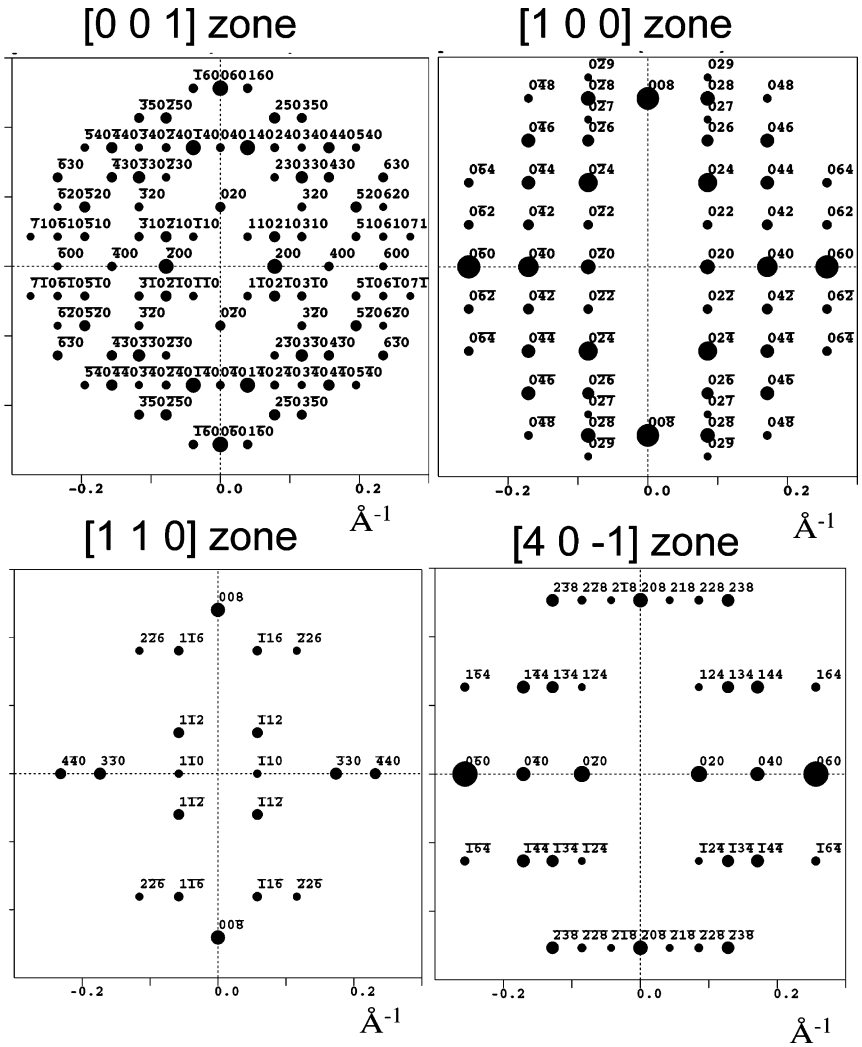

Figure 11. Calculated SAED patterns for various zone axes using the refined crystal structure of PFO (see Figure 10).

to ~5.2 Å vs 7.3 Å in the structure by Chen et al.[11] The 5.2 Å distance is too large to allow for significant π overlaps between adjacent PFO chains in the "dimer", which should prevent an efficient interchain transport in the crystal structure, as opposed to P3HT for which the π stacking distance between adjacent chains is ~3.8 Å. Each PFO dimer is surrounded by four dimers of opposite handedness. This peculiar arrangement of PFO chains having opposite handednesses is not unusual. It is observed in various polymer crystal structures, e.g., in the tetragonal structure of isotactic poly(4-methylpentene-1)[34] and in the orthorhombic structure (form III) of isotactic polybutene-1.[35] The originality of the present PFO structure stems from the fact that the handedness of the whole PFO chain is not related to the helical conformation of the backbone, but to the conformation of the lateral alkyl side groups. The difference in backbone chain conformation with respect to the nonplanar poly-(9,9-bis(2-ethylhexyl)-fluorene-2,7-diyl) probably results from the higher efficency of the packing of the longer *n*-octyl side chains in the trans conformation which are likely to favor interchain interactions in the PFO crystal. A similar effect of side-chain length on the backbone conformation has been reported in the case of poly(di-*n*-alkylsilane)s.[30]

(5) Origin of Epitaxy. The tentative structure proposed herein for PFO, showing an ordered packing of alkyl side chains, suggests an explanation based on epitaxy for the orientation of PFO on the TCB substrate. Indeed, as seen above, the oriented PFO films have a well-defined (1 0 0) contact plane on the (1 0 0) plane of TCB, i.e., $(1\ 0\ 0)_{PFO}||(1\ 0\ 0)_{TCB}$. Moreover, the PFO chains are oriented parallel to the *b*-axis of TCB, i.e., $b_{PFO}||c_{TCB}$. These observations strongly suggest that an epitaxial interaction is a play at the PFO/TCB interface. In the direction parallel to the PFO chains, a 3.8% mismatch is observed between the *b*-axis of TCB, namely $b_{TCB} = 0.395$ nm, and the 0.41 nm repeat distance between the layers of *n*-octyl side chains of PFO. A similar situation has been reported for P3HT oriented by directional epitaxial crystallization on TCB.[20,21] In the direction perpendicular to the PFO chain axis, a 12% mismatch is observed between $2b_{TCB} = 2.64$ nm and $b_{PFO} = 2.32$ nm. Even though this mismatch is still compatible with 2D epitaxy, we suggest that, similarly to P3HT, 1D epitaxy is at play in the case of PFO on TCB. The fact that PFO is readily oriented by epitaxy on TCB further supports the present crystal structure of PFO for which an ordered packing of the *n*-octyl side chains is proposed. Such a high level of orientation of PFO on TCB would be hardly compatible with a relatively disordered side chain structure as proposed by Chen et al.[11]

IV. Conclusions

This study has uncovered novel structure and morphology aspects of highly crystalline PFO thin films grown by directional epitaxial crystallization. First, PFO can be readily oriented, even without an underlying orienting substrate such as a rubbed polyimide, by using directional epitaxial crystallization with TCB as a solvent and substrate for epitaxy. This result

demonstrates that the method of directional epitaxial crystallization, recently used to orient various regioregular poly(3-alkylthiophene)s, can be extended to more rigid conjugated systems, e.g., polyfluorenes. The PFO chains are oriented parallel to the stacking direction of the TCB molecules (c_{TCB}). The thin films are composed of oriented nanocrystalline domains separated by grain boundaries. Both the crystallinity and the orientation of the films are effectively improved by annealing to 210 °C and slow cooling to room temperature. A new space group was identifed for the crystal structure of PFO, based on the indexation of representative SAED patterns obtained by electron diffraction and rotation-tilt experiments. PFO is found to crystallize in an orthorhombic unit cell and space group $Pnb2_1$. Simulations of the SAED patterns corresponding to different zone axes yields a tentative PFO chain conformation as well as positioning the PFO chains in the unit cell. A planar backbone conformation with a tetraradial configuration of the *n*-octyl side chains is proposed. Contrary to poly(9,9-bis(2-ethylhexyl)fluorene-2,7-diyl) which adopts a helical conformation, the ordered packing of the *n*-octyl side chains in the crystal is believed to enforce the planarization of the conjugated backbone of PFO. Moreover, we propose that the ordered packing of *n*-octyl side chains in the PFO structure is the *sine qua none* condition for its epitaxial orientation on TCB.

Acknowledgment. Enlighting discussions with Dr. Bernard Lotz and Dr. Marc Schmutz are gratefully acknowledged. C. Foussat is gratefully acknowledged for performing the GPC analysis of the PFO samples.

References and Notes

(1) Gather, M.; Bradley, D. D. C. *Adv. Funct. Mater.* **2007**, *17*, 479.
(2) Kline, R. J.; McGehee, M. D.; Kadnikova, E. N.; Liu, J.; Fréchet, J. M. J.; Toney, M. F. *Macromolecules* **2005**, *38*, 3319.
(3) Zen, A.; Pflaum, J.; Hirschmann, S.; Zhuang, W.; Jaiser, F.; Asawapirom, U.; Rabe, J. P.; Scherf, U.; Neher, D. *Adv. Funct. Mater.* **2004**, *14*, 757.
(4) Grice, A. W.; Bradley, D. D. C.; Bernius, M. T.; Inbasekaran, M.; Wu, W. W.; Woo, E. P. *Appl. Phys. Lett.* **1998**, *73*, 629.
(5) Grell, M.; Bradley, D. D. C.; Long, X.; Chamberlain, T.; Inbasekaran, M.; Woo, E. P.; Solimann, M. *Acta Polym.* **1998**, *49*, 439.
(6) Misaki, M.; Ueda, Y.; Nagamatsu, S.; Chikamatsu, M.; Yoshida, Y.; Tanigaki, N.; Yase, K. *Appl. Phys. Lett.* **2005**, *87*, 243503.
(7) Greenham, N. C.; Friend, R. H.; Bradley, D. D. C. *Adv. Mater.* **1994**, *4*, 491.
(8) Rothe, C.; Galbrecht, F.; Scherf, U.; Monkman, A. *Adv. Mater.* **2006**, *18*, 2137.
(9) Grell, M.; Bradley, D. D. C.; Ungar, G.; Hill, J.; Whitehead, K. S. *Macromolecules* **1999**, *32*, 5810.
(10) Winokur, M. J.; Slinker, J.; Huber, D. L. *Phys. Rev. B* **2003**, *67*, 184106.
(11) Chen, S. H.; Chou, H. L.; Su, A. S.; Chen, S. A. *Macromolecules* **2004**, *37*, 6833.
(12) Chen, S. H.; Su, A. C.; Su, C. H.; Chen, S. A. *Macromolecules* **2005**, *38*, 379.
(13) Chen, S. H.; Su, A. C.; Su, C. H.; Chen, S. A. *Macromolecules* **2006**, *39*, 9143.
(14) Chen, S. H.; Su, A. C.; Han, S. R.; Chen, S. A.; Lee, Y. Z. *Macromolecules* **2004**, *37*, 181.
(15) Redecker, M.; Bradley, D. D. C.; Inbasekaran, M.; Woo, E. P. *Appl. Phys. Lett.* **1999**, *74*, 1400.
(16) Grell, M.; Bradley, D. D. C.; Inbasekaran, M.; Woo, E. P. *Adv. Mater.* **1997**, *9*, 798.
(17) Sakamoto, K.; Usami, K.; Uehara, Y.; Ushioda, S. *Appl. Phys. Lett.* **2005**, *87*, 211910.
(18) Misaki, M.; Ueda, Y.; Nagamatsu, S.; Yoshida, Y.; Tanigaki, N.; Yase, K. *Macromolecules* **2004**, *37*, 6926.
(19) Wittmann, J.-C.; Smith, P. *Nature (London)* **1991**, *352*, 414.
(20) Brinkmann, M.; Wittmann, J.-C. *Adv. Mater.* **2006**, *18*, 860.
(21) Brinkmann, M.; Rannou, P. *Adv. Funct. Mater.* **2007**, *17*, 101.
(22) Miyaura, K.; Suzuki, A. *Chem. Rev.* **1995**, *95*, 2457.
(23) *Atlas of Polymer Morphology*; Woodward A. E., Ed.; C. Hanser Verlag: Munich, 1989; pp 106−111.
(24) Wang, W.; Lieser, G.; Wegner, G. *Macromoelcules* **1994**, *27*, 1027.
(25) Wang, W.; Lieser, G.; Wegner, G. *Liq. Cryst.* **1993**, *15*, 1.
(26) (a) Lieser, G.; Oda, M.; Miteva, T.; Meisel, A.; Nothofer, H.-G.; Scherf, U.; Neher, D. *Macromolecules* **2000**, *33*, 4490. (b) Knaapila, M.; Lyons, B. P.; Kisko, K.; Vainio, U.; Mihaylova, M.; Seeck, O. H.; Palsson, L.-O.; Serimaa, R.; Torkkeli, M.; Monkman, A. P. *J. Phys. Chem. B* **2003**, *107*, 12425. (c) Tanto, B.; Gusha, S.; Martin, C. M.; Scherf, U.; Winokur, M. J. *Macromolecules* **2004**, *37*, 9438.
(27) *International Tables of Crystallography*; Hahn, T., Ed.; Kluwer Academic Publishers: Dordrecht, 1989; Vol. A, pp 199−255.
(28) Chi, C.; Im, C.; Enkelmann, V.; Ziegler, A.; Lieser, G.; Wegner, G. *Chem.—Eur. J.* **2005**, *11*, 6833.
(29) Chi, C.; Lieser, G.; Enkelmann, V.; Wegner, G. *Macromol. Chem. Phys.* **2005**, *206*, 1597.
(30) (a) Miller, R. D.; Farmer, B. L.; Fleming, W.; Sooriyakumaran, R.; Rabolt, J. F. *J. Am. Chem. Soc.* **1987**, *109*, 2509. (b) Schilling, F. C.; Lovinger, A. J.; Zeigler, J. M.; Davis, D. D.; Bovey, F. A. *Macromolecules* **1989**, *22*, 3055. (c) Furukawa, S.; Takeuchi, K.; Shimana, M. *J. Phys.: Condens. Matter* **1994**, *6*, 11007.
(31) (a) Lovinger, A. J.; Davis, D. D.; Schilling, F. C.; Bovey, F. A.; Zeigler, J. M. *Polym. Commun.* **1989**, *30*, 356. (b) Patnaik, S. S.; Farmer, B. L. *Polymer* **1993**, *33*, 4443. (c) Takeuchi, K.; Furukawa, S. *J. Phys.: Condens. Matter* **1993**, *5*, L601. (d) Furukawa, S. *J. Organomet. Chem.* **2000**, *611*, 36.
(32) For additional information on the "clean" procedure used to refine the PFO chain conformation, see the *Cerius2 3.0 User's Guide on Modeling Environment*, pp 96−97 and pp 109, 110.
(33) Chunwachirasiri, W.; West, R.; Winokur, M. J. *Macromolecules* **2000**, *33*, 9720.
(34) De Rosa, C.; Borriello, A.; Venditto, V.; Corradini, P. *Macromolecules* **1994**, *27*, 3864.
(35) Cojazzi, G.; Malta, M.; Celotti, G.; Zannetti, R. *Makromol. Chem.* **1976**, *177*, 915.

MA071390D